An ESPI investigation of the crack-tip opening profile in brittle glass

Daniele Ferretti[1], Marco Rossi[2], Gianni Royer-Carfagni[1], Mirko Silvestri[3]

[1]*Dep. of Civil-Environmental Engineering and Architecture, University of Parma, Italy. E-mail*: *daniele.ferretti@unipr.it, gianni.royer@unipr.it*
[2]*Dep. of Civil Eng., University of Pisa, Italy. E-mail*: *marco.rossi2@studenti.unipr.it*
[3]*Consorzio Spinner, Bologna, Italy. E-mail*: *mirko.silvestri@gmail.com*

Keywords: glass, brittle fracture, Electronic Speckle Pattern Interferometry (ESPI), crack opening displacement (COD), stress concentration.

SUMMARY. The propagation of brittle fracture in annealed (float) glass has been observed with an Electronic Speckle Pattern Interferometry (ESPI) apparatus using coherent laser light. Specimens were first naturally pre-cracked at midspan with the sandwich-beam technique and, successively, tested under 3-P bending up to failure while measuring the displacement field and, in particular, the evolution of the crack opening displacement (COD) at the crack tip. By using a post-processing algorithm comparing 4 images lighted with phase-shifted laser beams, it has been possible to measure surface displacement far smaller than the wavelength of the illuminating light (532 nm), reaching a resolution of the order of 10 nm.

The transparency of glass has allowed to see that, right at the crack tip, the interface between sound and cracked material is not neat but curved and jagged, resembling a fractal surface. The measured COD at the specimen surface thus reveals a process zone at the crack tip where very large strains, rather than sharp separation, occur. Comparing the experimental results with the predictions of linear elastic fracture mechanics (LEFM), one finds that the measured crack-lips opening, left aside the process zone, is well fitted by the theoretical COD of a sharp straight crack, whose tip lies approximately in the middle of the process zone. By insight, the material tries to mitigate stress concentrations by producing this fractal boundary layer at the crack tip, with an effect equivalent to cohesive forces *à la* Barenblatt that bridge the crack lips.

1 INTRODUCTION

The molecular structure of glass consists of a geometrically irregular network of silicon and oxygen atoms with alkaline parts in between, and consequently has no slip planes or dislocations to allow for macroscopic plastic flow before fracture. This inability to yield plastically implies that glass remains linear elastic until fracture occurs ("brittle" response). Since the material strength is very sensitive to stress concentrations such as those induced by natural surface flaws, its accurate characterization must take into account the nature and behavior of such flaws.

Various models have been proposed to predict glass strength, but basically they are all based upon linear elastic fracture mechanics (LEFM), assuming sharp surface flaws in an elastic matrix and prescribing conditions for their growth under quasi-static loading [1]. Although the experience has confirmed that LEFM is a very reliable mathematical model for the lifetime prediction of glass integrity under applied loads, nevertheless the classical linear-elastic solutions imply the occurrence of infinite stress at the crack tip that, at least in principle, could overcome any material-strength threshold and in glass cannot be mitigated by plastic flow. The problem was ingeniously bypassed by Griffith [2], establishing crack equilibrium according to the well-known procedure of

energy balance. To overcome the somehow unrealistic finding of infinite stress at the crack tip, Dugdale [3] and Barenblatt [4-5] proposed the theory of cohesive cracks, in which cohesive forces are assumed to act at the edge of the crack lips in proximity of the crack tip. In the corresponding solution in linear elasticity theory the stress singularity is removed and the opposite edges of a crack result smoothly connected at each other at its ends.

We may wonder if in glass, and in brittle materials in general, cohesive forces are actually present and, if this is not the case, why the predicted stress singularity does not cause immediate failure whatever small the applied load is. Any experimental observation directed towards a better understanding of the phenomenon must consequently be able to evaluate the material deformation at the crack tip and, in particular, the crack opening displacement (COD). There are however major difficulties for such an experiment: the displacement at the crack tip should be measured with formidable precision (of the order of 1μm); on the other hand, fracture in brittle material is usually a catastrophic event, which requires high sensibility control devices and testing machines with real time feed-back response.

Here, we record the results of tests performed on glass beams, first naturally pre-cracked and successively brought up to rupture under bending in a closed-loop tensometer. An accurate and "continuous" measurement of the displacement field in a neighborhood of the crack tip has been obtained with a technique using a coherent laser-light referred to as Electronic Speckle Pattern Interferometry (ESPI) [6]. This method has been successfully used to analyze the fracture process in concrete [7] and metals [8], but to our knowledge this is the first time of its application to glass. The method consists in processing digital images obtained by lighting up the specimen with two distinct laser beams [6]: by using the phase-shifting technique [9], it is possible to evaluate "in plane" displacements of the order of 0.1 μm on a surface of 300x300 mm. From this measurement the crack profile has been accurately reconstructed and, moreover, the transparency of glass has allowed to take micrographs of the crack tip against the light. These have evidenced that the crack front is neither sharp nor straight; more in detail, the frontier between sound an fractured material is not neat but somehow faded in a "process zone" region, where the stress seems to be transmitted across a fractal-like surface. The measured COD has also been confronted with the prediction of classical LEFM. Comparing the experimental data with the theoretical COD of an equivalent sharp-crack, one finds an excellent agreement when the tip of the equivalent crack is approximately in the middle of the process zone.

The fact that material ligaments acting at a fractured zone in vicinity of the crack tip may possess a self-similar tortuosity, interpretable by a fractal fracture-surface, was proposed by Al. Carpinteri [10] to interpret the size-effect on tensile strength of brittle and disordered materials. Indeed, cracks with a smooth two-dimensional surface but with a fractal front can weaken the theoretical strength singularity predicted by LEFM [11]; in other words, the materials tries to accommodate the state of stress at the crack tip by developing a local loosening with self-similar characteristics.

2 THE TESTING APPARATUS AND THE EXPERIMENTAL PROGRAM

The ESPI technique [6] consists in comparing digital images obtained by lighting up the specimen with two distinct laser beams. The adopted ESPI equipment (Fig. 2.1) uses a 35mW NdYAG laser emitting a green light with wavelength λ=532nm. This is divided by a beam splitter into two beams, redirected by mirrors to the specimen surface after passing through lenses that spread the laser beam into spherically propagating waves, which can illuminate a 16cm x 16cm portion with intensity approximately 20μW/cm^2. The wave reflection on the rough specimen

surface and the interference of the two illuminating sources produces a green image characterized by speckles due to interference of the waves reflected with a random phase. This is the property on which the ESPI technique is based and its theoretical foundations are described for example in [6].

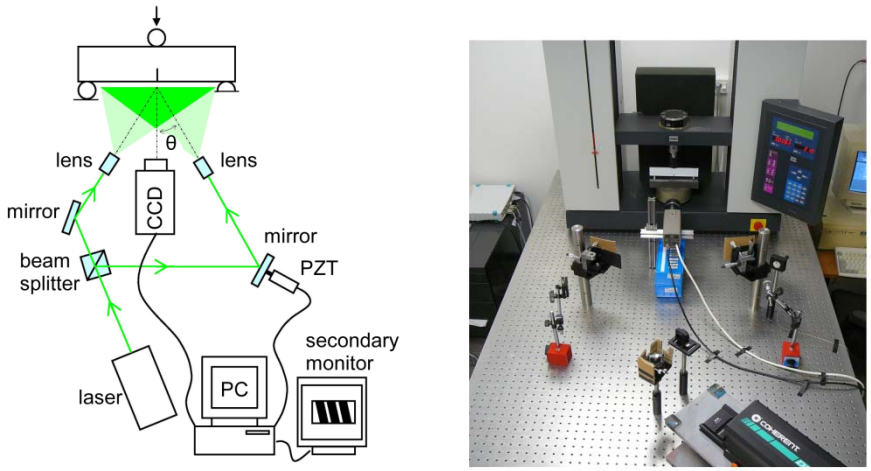

Figure 2.1 Experimental set-up: (a) ESPI optical scheme; (b) mechanical tensometer and optical device mounted on an air-floating table.

The image with speckles is captured by the CCD sensor of a camera and transferred to a PC through a frame grabber card with a resolution of 512×512 pixels at 256 gray levels, from black (dark) to white (saturation). Each image is then represented by a 512×512 matrix of integer numbers varying between 0 and 255, which represent the light intensity. The intensity I at a pixel depends upon the intensity of the two light beams on the specimen through the relation [6]

$$I = I' + I'' + 2\sqrt{I'\,I''}\cos\phi\ , \qquad (2.1)$$

where ϕ represents the phase difference between the two laser beams. The displacement of a point of the specimen produces a variation of the phase ϕ which can be related to the difference of the intensities measured before and after the deformation. On the whole specimen, this difference produces an image of interference fringes which is correlated with the component of displacement of a particle in the direction of the line corresponding to the intersection of the plane containing the two laser beams with the specimen surface. The fringed image is shown on a secondary monitor in order to follow in real time the evolution of the test.

In general, the resolution of optical techniques are limited by half of the wavelength of the lighting sources, but the ESPI is based upon differences in the laser light phases. Consequently, the resolution is much higher and can be further improved with the "phase-shifting" technique. This consists in capturing, at each step, four images, each one obtained by shifting the phase of one interfering laser beams of $\pi/2$. This shift is obtained by a nanometric translation (through a PZT actuator) of a mirror reflecting one of the beams (Fig. 2.1b). Denoting with I_1, I_2, I_3 and I_4 the pixel intensities corresponding to each of the four images and with φ the angle in $[0,\pi/2)$ such that $\tan\varphi = \left|(I_4 - I_2)/(I_3 - I_1)\right|$, if sgn(·) is the sign fuction (i.e., sgn(x) = {+1,0,–1} if x {>,=,<} 0), the

phase map is obtained by associating with each pixel the quantity

$$\Phi = \arctan 2\left(I_4 - I_2, I_3 - I_1\right) := \begin{cases} \operatorname{sgn}(I_4 - I_2)\cdot\varphi, & \text{if } (I_3 - I_1) > 0, \\ \operatorname{sgn}(I_4 - I_2)\cdot\pi/2, & \text{if } (I_3 - I_1) = 0, \\ \operatorname{sgn}(I_4 - I_2)\cdot(\pi - \varphi), & \text{if } (I_3 - I_1) < 0. \end{cases} \tag{2.2}$$

The function "arctan2" is a variation of the "arctan" function that produces results in the range $(-\pi,\pi]$, so that the map that is obtained may be discontinuous modulo 2π. From the difference between phase maps calculated at the beginning and at the end of each load step we obtain a fringe image which represents the relative phase, modulo 2π, due to the displacements of the surface of the specimen. The typical grainy speckle images are processed with specific filters. At this point, we need to pass from the phase map modulo 2π to a continuous phase map, with grey tones: this can be done by using a post-processing known as "phase unwrapping". For the case at hand, the explicit unwrapping algorithm is that proposed by Flynn [12]. Finally, from the continuous phase map, the map of relative displacements Δu, i.e., the displacement of a particle corresponding to the compared states to which the images refer to, can be obtained through the equation

$$\Delta u = \frac{\lambda\Phi}{4\pi\sin\theta}\ , \tag{2.3}$$

where θ is the angle between the laser beam and the normal to the specimen surface (Fig. 2.1a). With this procedure, displacements can be evaluated with a resolution of 0.01 μm for a maximum value of about 5 μm. Indeed, the displacements of the specimen are much larger, and for this reason it is necessary to apply sufficiently small load steps, updating the initial image at each step. The total displacement u is obtained as the sum of the displacements Δu measured at each step. Of course, the smaller the loading step, the more accurate the measure.

Figure 2.2 Sandwich beam apparatus used to naturally pre-crack the glass specimens.

Four prismatic beams were tested, approximately 200mm × 39mm × 5.9mm, all made of annealed soda-lime float glass and here referred to as specimens A, B, C and D. Using a diamond saw they were initially pre-notched in the middle (notch approximately 10mm deep and 1mm wide) and successively loaded in 3P bending with the sandwich beam technique proposed in [13], This is represented in Fig. 2.2: the glass specimen is encompassed by two external aluminum beams, that constrain the glass beam so that a stable natural crack can be formed. A difference with respect to [13] was the use of 1.52mm-thick ionoplast-polymeric spacers between aluminum

and glass, fitted in place after mollification through heating, which efficiently avoided stress concentration in glass at the contact points. The measured height of the natural crack so formed was 8mm, 16mm, 5 mm and 4mm for specimens A,B,C and D, respectively.

In order to reflect the laser light, the specimens had to be made opaque. Therefore, specimens A and B were sprayed with a white acrylic paint. This layer was very thin but elastic so that, even if its strength was certainly negligible, it did not completely fractured when the underlying glass cracked, thus bridging the crack lips at the tip. The bridging effect was reputed negligible, but to prove this ruling out any doubt, specimens C and D were just colored with a green felt-tip permanent marker pen. Unfortunately, the specimens remained at least partially transparent, thus spoiling a little the ESPI images.

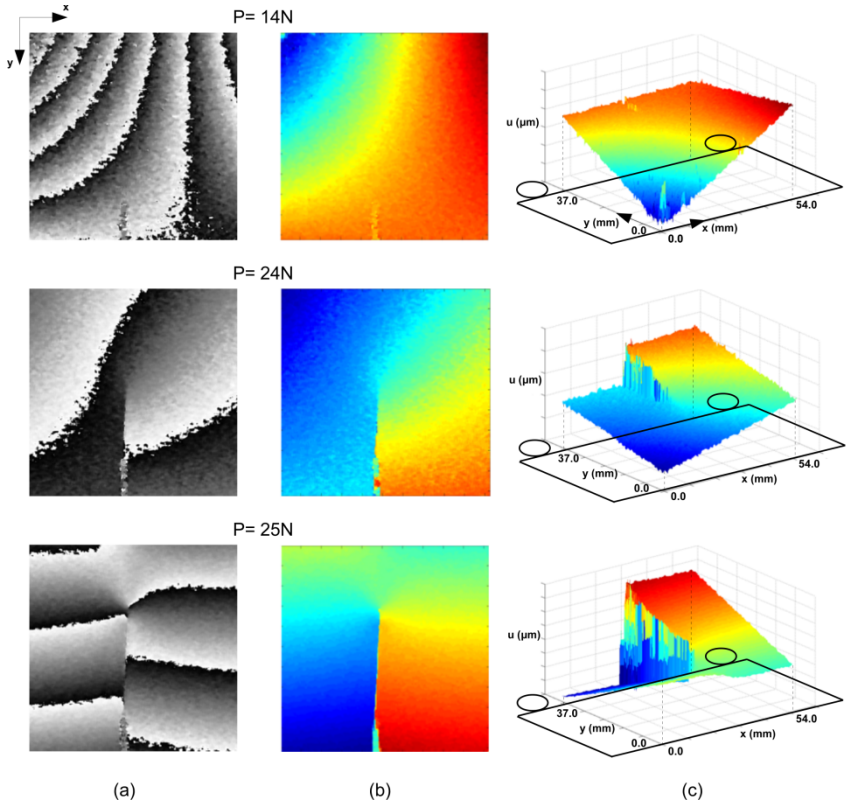

Figure 3.1 Experimental measurements of crack propagation at various load levels (specimen A): (a) phase maps; (b) unwrapped phase maps; (c) horizontal component of the displacement field.

3 EXPERIMENTAL RESULTS

The phase-map (modulo 2π) images obtained with the ESPI are shown in Fig. 3.1a for a paradigmatic case (specimen A) under three different loads. Here each pixel corresponds to a rectangular portion of the specimen surface of about 98μm × 70μm; the fringe discontinuity reveals the widening of a crack. Fig. 3.1b shows instead the unwrapped phase maps, where it is possible to note the prenotch and the crack propagation. The 3D plot of the corresponding horizontal (in the x direction) component of displacement $u(x,y)$ is reported in Fig. 3.1c. The

evident jump in the resulting surface is associated with the crack opening displacement, increasing with increasing load. The intersection of the surfaces of Fig. 3.1c with planes orthogonal to the *y* axis gives the horizontal displacement profiles for longitudinal horizontal fibers of the glass beam. These are plotted in Fig. 3.2 for 4 different heights *y*. Notice that in the upper (uncracked) portion the glass beam (section A in Fig. 3.2) the displacement is continuous. Approaching the crack tip (section B in Fig. 3.2), the displacement is still continuous, but it is possible to note a variation in the slope of the graph which represents a strain concentration. Further lowering the reference fiber (section C in Fig. 3.2) the displacement now exhibits a jump, which corresponds to the crack width w at the considered level.

Unfortunately, due to the background noise in the acquired images, it was not possible to measure the crack width directly. We then adopted the following strategy. The two portions of the displacement graph on the l.h.s. and the r.h.s. in a neighborhood of the crack zone were interpolated by two lines using the least squares method; the distance between these lines, measured in the direction of the ordinate axis, was associated with the crack opening w (Fig. 3.2d). By measuring w at different heights *y*, it was then possible to reconstruct the crack opening displacement. Figs. 3.3 show the evolution at increasing load of the COD for the four specimens A, B, C and D: these graphs have a conventional significance because the crack-lips have been plotted symmetric, even if there is no experimental evidence of this symmetry. In general we observed that specimens coated with the white spray (A and B) produced less noise than the specimens colored with the green felt-tip marker (C and D) and, moreover, the crack propagation was less brittle in the former ones than in the latter ones, because of the crack bridging effect of the paint layer. Notwithstanding, the shape of the crack profile is similar in all the four cases.

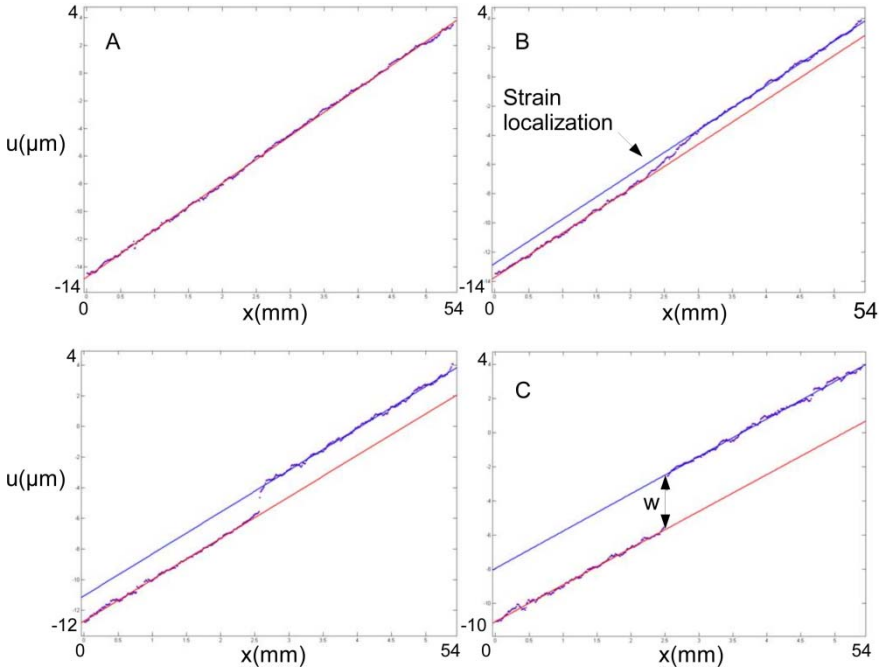

Figure 3.2 Horizontal component of displacement on horizontal fibers at various heights (Specimen A).

Notice that in proximity of the maximum of each graph in Fig. 3.3, a dashed curve has been reported. This corresponds to a region where the displacement plot is similar in type to that of Fig. 3.2b. Here a strain "concentration", rather than a sharp displacement jump, occurs, but the dashed curve corresponds to the profile of a "fictitious crack", whose opening has been calculated by measuring the distance between the two lines interpolating the l.h.s. and r.h.s. portions of the displacement graph (Fig. 3.2), as mentioned above. This zone is actually the "process zone" where the crack is nucleated.

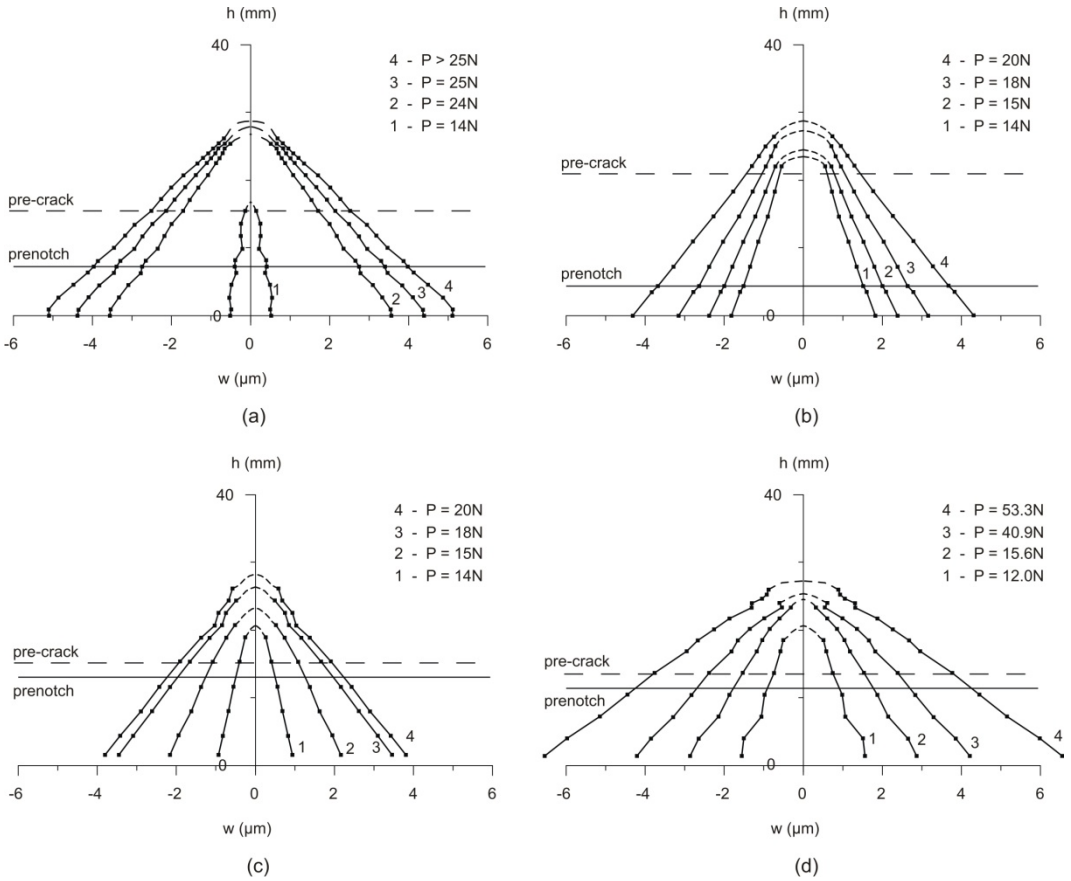

Figure 3.3 Crack-Opening-Displacement (COD) at various load levels: (a) specimen A; (b) specimen B; (c) specimen C; (d) specimen D. Axes differently scaled: Height "h" in mm and crack opening "w" in μm.

Indeed, the transparency of glass has allowed to take micrographs of the crack tip against the light. These have evidenced that the crack front is not straight by kinked almost symmetrically with respect to the specimen middle plane (Fig. 3.4). More in detail, the frontier between sound an fractured material is not neat but somehow faded in the "process zone", where the stress seems to be transmitted across an imaginary "fractal" surface [10]. In general, we have observed that the characteristic size of this interface region does not depend upon the crack length.

4 DISCUSSION AND CONCLUSIONS

It is well-known that LEFM predicts that the COD in a neighborhood of a straight-sharp-crack tip under mode-*I* loading in generalized plane stress, is of the form [14]

$$\mathrm{COD} = 4\left(\frac{2}{\pi}\right)^{1/2} \frac{K_I}{E} r^{1/2} \,, \tag{4.1}$$

where K_I is the stress intensity factor, E is the Young's modulus and r represents the distance from the tip measure along the crack. For a beam of length L loaded by P in 3-P bending, the expression for K_I may be expresses in a series of the form

$$K_I = \frac{PL}{t\,h^{3/2}}\left[2.9\left(\frac{a}{h}\right)^{1/2} - 4.6\left(\frac{a}{h}\right)^{3/2} + 21.8\left(\frac{a}{h}\right)^{5/2} + o\left(\frac{a}{h}\right)^{5/2}\right] \,, \tag{4.2}$$

where t and h are the specimen thickness and height, while a is the depth of the crack (Fig. 4.1).

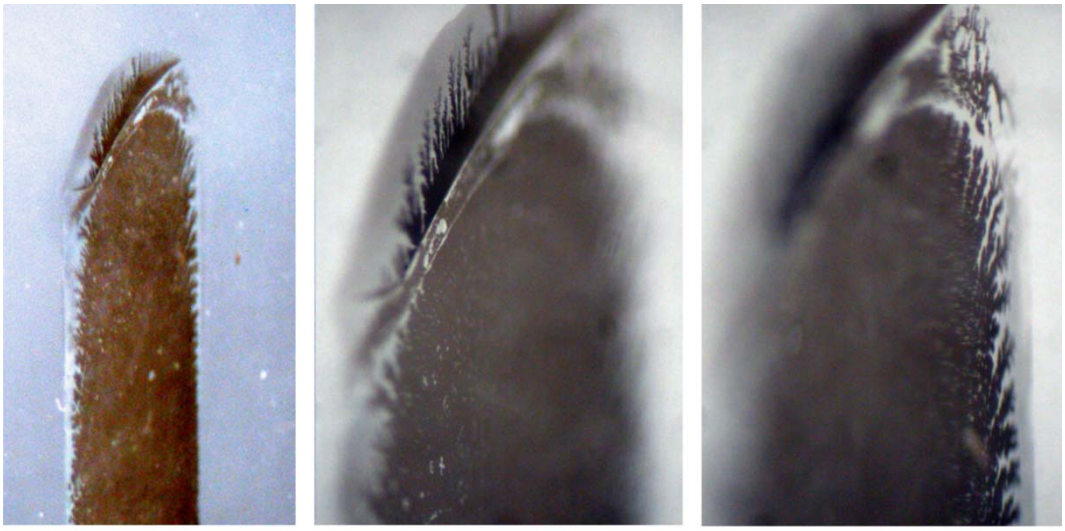

(a) (b) (c)

Figure 3.4. Crack tip observed against the light with an optical microscope. Since optical depth of field is reduced, the three pictures bring into focus different details.

A comparison can be made between the experimentally-observed wiggly and curved crack (sketched on the l.h.s. of fig. 4.1) and an ideal straight sharp-crack (r.h.s. of fig. 4.1), by comparing the experimental COD for the former with the theoretical LEFM prediction for the latter. Of course, as schematically represented in Fig. 4.1, the tip of the straight sharp crack, indentified by the parameter a in (4.2), should lie in fractal-like process zone. Trying to fit the measured COD with the LEFM prediction of (4.1), one finds an excellent agreement when the tip of the equivalent sharp crack is approximately in the middle of the process zone (Fig. 4.1).

The considerations which follow can only be considered conjectural at this time, but it is expected that they may confirmed, at least partially, by further research. The presence of the fractal-like process-zone (Fig. 3.4) somehow mitigates the stress state that in a sound material with

a perfectly sharp crack would become unboundedly large [11]. In the process zone the material is neither sound nor fractured, in the sense that the strain tends to localize but the material can still support a non-zero stress. This effect could be modeled by introducing cohesive forces *à la* Barenblatt [4-5], bridging the crack lips in a very small neighborhood of the crack tip.

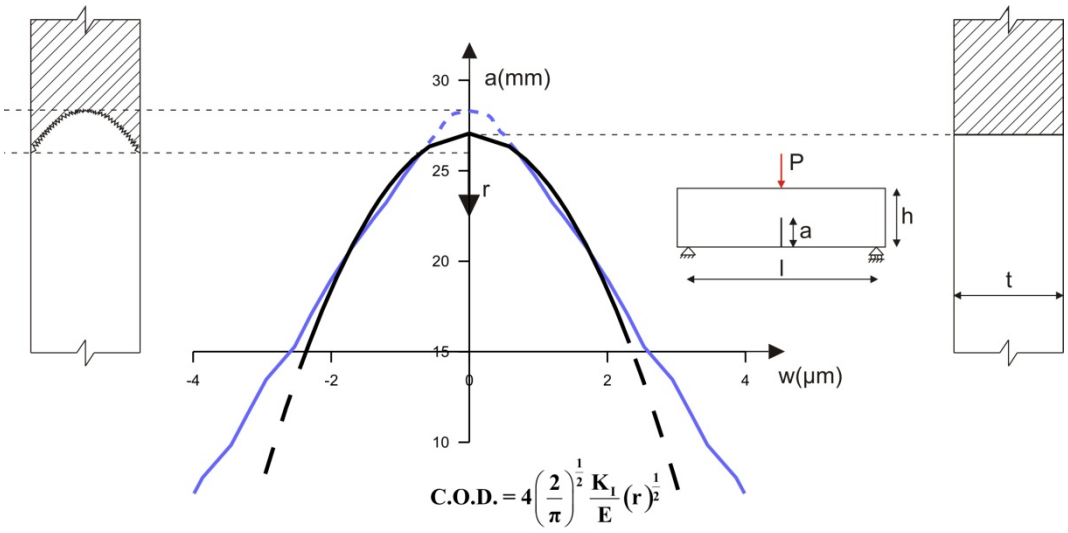

Figure 4.1. Equivalence between the observed wiggly crack, on the l.h.s., and a straight crack, on r.h.s.. Comparison between the experimental COD of the former with the theoretical LEFM prediction for the latter.

The basic assumptions of Barenblatt's theory of equilibrium cracks are essentially three: *i*) the longitudinal size of the cohesive end-region is small compared with the size of the entire crack; *ii*) the intensity of the cohesive forces and the size of the end-regions are independent from the applied loads (or, equivalently, the relative displacement of the surface points of the end region does not depend upon the applied loads and is always the same for a given material); *iii*) the stress remains finite at the end of the crack (or, equivalently, the opposite edges of a crack are smoothly connected at each other at its ends). From these hypotheses, in particular from *i*), it can be verified [4-5] that at points sufficiently far away from the crack tip the displacement produced by cohesive forces are small if compared with those produced by the basic applied loads, whereas cohesive forces determine the displacement just in the vicinity of the crack end, producing the smooth connection of the opposite edges. In other words, *close* to the crack-end but not *at* the crack-end, the COD coincides with that predicted by LEFM.

Observations at the microscope of the fractured glass specimens have provided evidence that the characteristic size of the process zone is very small if compared with the size of the entire crack. Moreover, the equivalence established as *per* fig. 4.1. indicates that *close* to the crack-end, but outside the process zone, the measured COD squares surprisingly well with the theoretical COD of a sharp crack whose tip is approximately in the middle of the process zone. It is impossible not only to measure but also to define the COD inside the fractal-like process zone, but

it is presumable that inside this region the stress is not infinite but attains at all points a threshold value comparable with the local strength of the material. In conclusion, in glass there are no definite smoothly-connected crack lips in the end-region, but nevertheless the effects are substantially similar to those described by Barenblatt's theory.

Indeed, classical LEFM may furnish a good first-order approximation through the equivalence described in fig. 4.1. However, when complex phenomena in the glass response (static fatigue, crack annealing, influence of surface flaws) have to be considered [1], it would be desirable to resort to more sophisticated models that take into account the presence of the process zone.

ACKNOWLEDGEMENTS

This research was partially supported by the Italian MURST under the program PRIN 2005 "Affidabilità di elementi in vetro strutturale: indagini teoriche e sperimentali sulla risposta termo-meccanica del materiale e di strutture trasparenti di tipo innovativo".

References

[1] Haldimann, M., Luible, A. and Overend, M., *Structural use of Glass*, IABSE-AIPC-IVBH Pub., Zurich (2008).

[2] Griffith, A. A., The phenomenon of rupture and flow of solids, Phil. *Trans. Royal Soc. London*, **A221**, 163-198 (1920).

[3] Dugdale, D. S., Yielding of steel sheets containing slits, *J. Mech. Phys. Solids*, **8**, 100-108 (1960).

[4] Barenblatt, G.I., The formation of equilibrium cracks during brittle fracture: general ideas and hypotheses. Axially symmetric cracks, *Prikl. Mat. Mech.*, **23**, 622-636 (1959).

[5] Barenblatt, G.I., The mathematical theory of equilibrium cracks in brittle fracture, *Adv. Appl. Mech.*, **7**, 55-129 (1962).

[6] Jones, R. and Wykes, C., *Holographic and Speckle Interferometry*, Cambridge Studies in Modern Optics, Cambridge University Press, Cambridge (1989).

[7] Jia, Z. and Shah, S.P., Two-dimensional electronic-spleckle-pattern interferometry and Concrete-fracture processes, *Experimental Mechanics*, **34**, 262-270 (1994).

[8] Yoshida, S., Muhamed, I., Pardede, R., Widiastuti, R., Muchiar, G., Siahaan, B. and Kusnowo, A., Optical interferometry applied to analyze deformation and fracture of aluminum alloys, *Theoretical and Applied Fracture Mechanics*, **27**, 85-98 (1997).

[9] Creath, K., Phase-shifting speckle interferometry, *Applied Optics*, **24**, 3053-3058 (1985).

[10] Carpinteri, Al., Fractal nature of material microstructure and size effects on apparent mechanical properties, *Mechanics of Materials*, **18**, 89-101 (1994).

[11] Cherepanov, G.P., Balankin, A.S. and Ivanova, V.S., Fractal fracture mechanics – A Review, *Engineering Fracture Mechanics*, **51**, 997-1033 (1995).

[12] Ghiglia, D.C. and Pritt, M.D., *Two dimensional phase unwrapping - Theory, algorithms and software*, John Wiley and Sons, New York (1998).

[13] Sglavo, V.M., Bosetti, P., Trentini, E. and Ceschini, M., Sandwiched-beam procedure for precracking brittle materials, *Journ. of the Am. Ceramic Society*, **82**, 2269- 2272 (2004).

[14] Carpinteri, Al., *Scienza delle Costruzioni vol. 2*, Pitagora Editrice, Bologna (1992).